HAL open science

Characterization of low and high frequency phenomena in a PEM fuel cell using singularity analysis of stack voltage

Djedjiga Benouioua, Denis Candusso, Fabien Harel, Xavier Francois, Pierre Picard

To cite this version:

Djedjiga Benouioua, Denis Candusso, Fabien Harel, Xavier Francois, Pierre Picard. Characterization of low and high frequency phenomena in a PEM fuel cell using singularity analysis of stack voltage. Journal of Energy Storage, 2020, 28, pp.32. 10.1016/j.est.2020.101298 . hal-02492847v2

HAL Id: hal-02492847

https://hal.science/hal-02492847v2

Submitted on 10 Mar 2020

HAL is a multi-disciplinary open access archive for the deposit and dissemination of scientific research documents, whether they are published or not. The documents may come from teaching and research institutions in France or abroad, or from public or private research centers.

L'archive ouverte pluridisciplinaire **HAL**, est destinée au dépôt et à la diffusion de documents scientifiques de niveau recherche, publiés ou non, émanant des établissements d'enseignement et de recherche français ou étrangers, des laboratoires publics ou privés.

Characterization of low and high frequency phenomena in a PEM fuel cell using singularity analysis of stack voltage

Djedjiga Benouioua[1,2,3,*], Denis Candusso[1,2,3], Fabien Harel[3,4], Xavier François[3,5], Pierre Picard[1,6]

[1] ITE EFFICACITY, 14-20 Boulevard Newton, Champs-sur-Marne, F-77447 Marne la Vallée, France.
[2] Université Gustave Eiffel, IFSTTAR / COSYS, SATIE (UMR CNRS 8029), 25 Allée des marronniers, F-78000 Versailles Satory, France.
[3] FCLAB, FR CNRS 3539, Rue Ernest Thierry Mieg, F-90010 Belfort Cedex, France.
[4] Université Gustave Eiffel, Université de Lyon, IFSTTAR / AME / ECO7, 25 Avenue François Mitterrand, Case24, F-69675 Bron Cedex, France.
[5] UTBM, Rue Ernest Thierry Mieg, F-90010 Belfort Cedex, France.
[6] ENGIE - CRIGEN, 361 Avenue du Président Wilson BP 33, F-93211 La Plaine Saint-Denis, France.

[*] Corresponding author: djedjiga.benouioua@utbm.fr

Abstract:
The aim of this work is to propose a new development of the fuel cell characterization tool based on Voltage Singularity Spectrum (*VSS*), a pattern that can advantageously be estimated from the "free" evolution of the stack voltage. A Polymer Electrolyte Membrane Fuel Cell (*PEMFC)* designed to operate in micro Combined Heat and Power units is investigated to create an experimental database made of normal and abnormal operating conditions. Some *VSS* signatures based on Wavelet Leader Multifractal Analysis (*WLMA*) are computed on low- and high-frequency filtered stack voltage signals reflecting different physical phenomena dynamics. The resulting low- and high-frequency *VSS* computed for six different operating conditions are then compared to the Electrochemical Impedance Spectra (*EIS*) recorded in the same conditions. In this way, we intend to establish some links between the *VSS* patterns and the *EIS* based on well-known physical analyses. We also show that the dominant singularity strengths of the low (and possibly also high) frequency *VSS* can be considered as relevant clustering features to identify various *PEMFC* operating states (linked with poorer / better air diffusion, with lower / higher *MEA* hydration), as it is usually done with the use of the characteristic resistances intercepted on the *EIS* graph x-axis.

Keywords: Hydrogen; Fuel Cell; Diagnostic; Singularity analysis; Electrochemical Impedance Spectroscopy; Micro-cogeneration

Paper contents:

Paper contents: 2
Nomenclature: 3
1. Introduction 4
2. Experimental 8
2.1. Description of the investigated PEMFC stack 8
2.2. Testbench architecture description 9
2.3. PEMFC test protocol 10
3. How to build the low- and high-frequency *VSS* signatures? 13
4. *VSS* - *EIS* comparisons and use of pattern parameters for diagnostic purpose 18
5. Conclusions 25
Acknowledgments: 26
References: 27
Figure captions: 30
Table captions: 32

Nomenclature:

μCHP	Micro Combined Heat and Power
CO_2	Carbone dioxide
D(h)	Hausdorff dimension
EIS	Electrochemical Impedance Spectrum
FC	Fuel Cell
f_s	Sampling frequency (Hz)
λa	Factor of Stoichiometry at Anode
λc	Factor of Stoichiometry at Cathode
h	Hölder exponent
h_0	Dominant singularity strength
H_2	Hydrogen
Hf	High frequency
Hf-Re(Z)	High frequency resistance
Hf-VSS	High Frequency Voltage Singularity Spectrum
I	Current (A)
Im(Z)	Imaginary part of the impedance *Z* in the Nyquist diagram (EIS plot)
j	$j^2 = -1$
Lf	Low frequency
Lf-Re(Z)	Low frequency resistances
Lf-VSS	Low Frequency Voltage Singularity Spectrum
MEA	Membrane Electrode Assembly
N	Filter order
O_2	Oxygen
OC	Operating Condition of the fuel cell
PEMFC	Polymer Electrolyte Membrane Fuel Cell
Re(Z)	Real part of the impedance *Z* in the Nyquist diagram (EIS plot)
Ref	Reference operating conditions
RH	Relative Humidity
SoH	State-of-Health.
SS	Singularity Spectrum
T	Temperature of the fuel cell (°C)
VSS	Voltage Singularity Spectrum
WLMA	Wavelet Leader based Multifractal Analysis
ω, ω_c	Angular frequency, cutoff frequency (rad / s)

1. Introduction

Considerable worldwide attention has recently been focused on decentralized power stations and individual household generators based on Fuel Cell (*FC*) units fed with natural gas as fuel and energy storage medium. In particular, Japan has expended substantial effort in developing the ENE-FARM project, which hits around 140 000 residential thermoelectric *FC* generators with an ambition to reach 1.4 million units by 2020 and 5.3 million by 2030 [1]. In Europe, decentralized power generator technologies have been supported by two major programs: the CALLUX German project (2008-2016) involving approximatively 800 *FC* heating appliances installed in individual households [2], and the ENE FIELD project (2012-2017), which deployed up to 1000 thermoelectric *FC* systems for the residential sector in 11 European countries [1, 3].

Polymer Electrolyte Membrane Fuel Cell (*PEMFC*) is considered as a really promising energy system for decentralized power production, as a substitute for conventional technologies for the tertiary sector (e.g. Combined Heat and Power - *CHP* [4, 5]; also called cogeneration). Small scale *FC* systems, named μCHP (or micro cogeneration), with typical power range less than 50kW for power and heat generation are dedicated to residential and tertiary sector buildings [6]. The main advantage of a *PEMFC* system lies in its high energy conversion efficiency. For example, Panasonic claims that its 2015 model achieves 95% combined heat and electrical efficiency [7], and brings forward its capability to reduce environmental impacts shown by low pollutant and acoustic emissions. The possibility to be used for cogeneration applications and to exploit reforming processes allows the use of more traditional / conventional fuels and/or bio fuels as energy storage media (e.g. natural gas, methanol, biogas, biohydrogen, etc. [8, 9]), proving high flexibility and achieving a reduction in the number of required external components [7].

Despite of the desirable properties cited above, one of the primary barriers to achieve widespread commercialization of *PEMFC* systems is the durability, which is one of the most important issues to be addressed in the various industrial sectors [10]. Indeed, *FC* lifespan increase becomes a predominant challenge in research and industry, ranging from 5000 operating hours for car applications (20000 hours for bus applications) to 40000 - 70000 operating hours for stationary applications. For example, Panasonic showcased a prototype of a hydrogen *FC*, under development in the framework of its new ENE FARM project, with a lifetime of 70000 hours [7].

To achieve these durability and reliability targets, it is essential to monitor the State of Health (*SoH*) of the *FC* system during its operation in the application environment. Numerous works dealing with this issue can be found in the literature. These works aim to improve the *PEMFC* performances as well as to increase the durability by proposing relevant diagnosis techniques and strategies. The model-based approaches [11-14] are part of these techniques. They are very cumbersome and complex because they require an in-depth knowledge of the multi-physical mechanisms (thermal, electrical, electrochemical, and fluidic ones) and they are based on numerous parameters governing the operation of a *FC* system.

Hence, more and more attention is paid to data-driven techniques [15-17] because of their simplicity regarding the implementation and the good performances obtained, without deep system structure knowledge and achieved by efficient signal processing methods as: Fourier transform [18], multi-resolution analysis [19], singularity analysis [20-25]. For fault identification and isolation tasks, some works use Electrochemical Impedance Spectra (*EIS*) [26] as normal or faulty operation signatures to supply artificial intelligence algorithms (based for instance on fuzzy logic [27] or neural networks [28]) or conventional pattern recognition approaches (based on Support Vector Machines (*SVM*) [29], k-nearest neighbors (*knn*) methods) [20, 22].

At the same time, some specific efforts are devoted to the development of non (or less) invasive measurement tools to collect some useful data for the *FC* diagnosis algorithms. In [30], Rubio et al. provide a good overview of these methods. Some of them (e.g. neutron imaging techniques to investigate the water distribution, magnetic field sensors external to the *FC* to measure the local current density distributions) require some complex equipment and significant expenses that cannot be incorporated into actual *FC* system operations. A more elegant, non-invasive approach is to listen to the electrochemical device, recording and analyzing the noise generated [18, 30]. Especially the *FC* voltage noise shall be collected and analyzed because the generator is expected to include a cell or a stack voltage monitoring system.

In [30], the diagnosis of *PEMFC* (single cell equipment with an electrode surface of 50 cm²) is explored by comparing Fourier and wavelet transform analyses of cell voltage noise to electrochemical impedance data. The experimental noise data are collected for a range of air Relative Humidity (*RH*) and stoichiometry rates including conditions leading to electrode flooding, membrane dehydration and air starvation failure modes. The noise data are recorded in every experiment during 300 s but only the last 50 s are considered in the signal processing analyses. This 50 s time window is found to be large enough to estimate the cell state. The main conclusion of the work is that the wavelet transform procedure is preferred to Fourier analysis because it is suitable for real-time use and yields a relatively greater sensitivity to operating condition variations. The authors indicate also that the changes in the wavelet coefficient standard deviations for selected noise frequencies are sufficient to reconstruct the original *FC* operating conditions state.

In [18], Maizia et al. develop a methodology of spectral analysis and evaluate the possible non-stationarity character of a *PEMFC* voltage signal to investigate some water management issues. The experiments are conducted on a single cell with an electrode area of 25 cm² and by applying three current levels (0 A, 2.5 A, and 8 A). According to Maizia et al., the data acquisition for each operating point needs to be performed during 2 h to obtain a clean and rich signal, especially at low frequency. Some power spectral density of voltage fluctuations are then calculated using Fast Fourier Transform. The results obtained indicate that the power spectral density can be used for the detection of an incorrect *FC* water balance (especially, in drying conditions with low RH rates of 20% at anode and cathode).

To monitor and diagnose the *PEMFC* system *SoH*, we propose to use an innovative data driven approach that is the singularity analysis. This method consists in analyzing the morphology of the *FC* voltage signal, monitored at the stack terminals, and more precisely the pointwise singularities stamped in the signal recorded for various operating conditions. The singularity features of the voltage are then summarized in the form of concave arcs estimated thanks to a set of mathematical equations, known as the multifractal formalism [20-25]. Each arc is a plot of the fractal dimension *D(h)* vs. the Hölder exponent *h*. Building a singularity spectrum consists in associating to each Hölder exponent h the Hausdorff dimension *D(h)* of the sets of points which exhibit the same value of *h*.

This advanced analysis tool, named Voltage Singularity Spectrum (*VSS*), has multiple interests. First, the tool is based on a thorough analysis of the sole stack voltage roughness. It is not required to monitor any other *FC* operating parameters while other signal-based diagnosis strategies might be based on the measurement of additional physical values, as the gas pressure drop at cathode for instance [19]. Moreover, we have already shown that the *VSS* tool can be used with a complete stack (i.e. an assembly of individual cells), and not only with a single electrochemical cell [18, 30]. Nor is it necessary to monitor the individual cell voltages in the stack to make the diagnosis, as it is the case for instance with a diagnosis based on statistical approaches and individual cell voltage distributions. Second, the tool is obtained using a non-intrusive manner and without affecting in any way the *FC* operation; only the "free" evolution of FC stack voltages is considered. Indeed, no external additional AC-excitation has to be superimposed to the existing DC load current as it is the case in the usual *EIS* operation mode; no accurate controls of FC current or voltage and thus no additional and expensive equipment (e.g. electrochemical impedance spectrometer) are required.

A first version of the voltage singularity analysis method was described in [21]. The computing of the *VSS* was based on continuous wavelet transform applied to a stack voltage recorded at a frequency close to 11 Hz. The characterization of various *FC* operating states through the multifractal formalism was applied to an 8-cell stack designed for automotive applications and fed with pure hydrogen. A preliminary comparison between *VSS* patterns and *EIS* signatures was proposed for four different operating conditions. The design of a complete *FC* diagnosis strategy was proposed, including its different steps, namely: signal acquisition, signature calculations, and classifications of the FC operating states (using pattern recognition methods as *SVM* and *knn*). The results of such a *FC* diagnosis strategy (including an additional step of optimal *VSS* feature selection technique) applied to the 8-cell stack data base were published in [22]. The faults considered (variations of gas stoichiometry rates, of gas pressure level, stack temperature, CO content in the fuel) were quite simple as no combination of faults (i.e. by considering two or more failures simultaneously during the *FC* operation) was considered.

A second version of the voltage singularity analysis method was described in [23]. In this case, the multifractal analysis was based on wavelet leaders with the aim to ensure a more rapid and efficient computing of the *VSS*. The method was still applied to an 8-cell stack voltage recorded at a frequency

close to 11 Hz. The proposed *PEMFC* diagnosis tool allowed identifying simple operating failure cases and even more complicated situations that contain several failure types. In [24], we could show that the dynamic multifractality of the stack voltage can also be considered as a relevant tool for the monitoring of the FC aging state. The computed *VSS* patterns were compared with *EIS* signatures recorded at three-time intervals of a 124 h aging test. However, only the low frequency shapes of the *EIS* signatures could be considered in the comparisons since the *VSS* were still calculated from stack voltages recorded at 11 Hz. The portability of a diagnosis strategy based on *VSS* features and machine learning approaches was examined in [25] by considering two 11 Hz test databases collected with two different *PEMFC* stacks. The first assembly was designed for automotive applications and fed with pure hydrogen while the second one was dedicated to stationary use (μCHP application) and fed with a mixture of hydrogen and CO_2, simulating a reformat produced from natural gas.

In this paper, we present a new development of the *VSS* technique dedicated to the voltage monitoring and diagnosis of *PEMFC* stacks. This development is based on an experimental campaign conducted with a *PEMFC* stack, fed by a H_2 & CO_2 fuel mix simulating a reformat and operated in various conditions. More details on the data measurement and collection will be given in Section 2. In the presented work, we operate this database, and continue to estimate and use the *VSS* characterization tool, which is based on a thorough analysis of the sole stack voltage roughness and offers useful information on the stack *SoH*, summarized through a concave curve that can be compared with the *EIS* popular analysis tool. The *VSS* characterization tool is intended to distinguish between different *FC* operating conditions in the framework of a diagnosis strategy whose principle is illustrated in Fig. 1 and relies on two basic steps. The first step deals with the voltage signal analysis. It contains two analysis blocks (signal filtering and singularity computation). The new tool developed in this work leads to a deep analysis of the stack voltage signal by separating the high and low frequency components of the signal, which correspond to high and low frequency dynamics of physical phenomena occurring in the *FC* assembly. The proposed analysis method consists of computing singularity measurements on the filtered voltage signals. The raw signals are recorded at a frequency of 3 kHz for different operating conditions (normal and abnormal ones) and, in this new approach, *VSS* are computed for two frequency levels. The second step of the diagnosis strategy shown in Fig. 1 explores the machine-learning field in order to detect and isolate *FC* faults. Throughout this article, we will further develop the two analyses blocks linked with the step 1 of the diagnostic strategy. The two signal processing blocks will be described in Section 3.

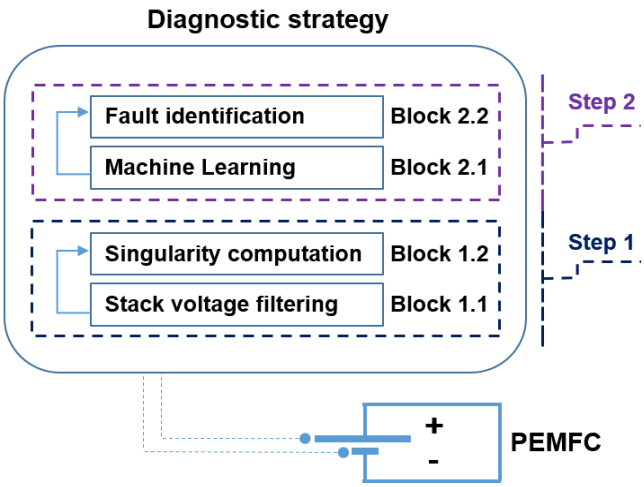

Fig. 1. Synoptic diagram illustrating the two different steps of the proposed diagnostic strategy. This article deals with the step 1 of the global approach.

The article also aims to highlight any possible relations existing between *VSS* and *EIS* signatures, and we will indicate how *VSS* parameters (e.g. dominant irregularity *h0* of the *VSS* computed at low and high frequency) could be used for diagnostic purpose, like it can be done using any parameters of the EIS patterns (e.g. membrane and polarisation resistances.) The results obtained through the *VSS* signatures will be discussed and compared with *EIS* records in Section 4. Finally, major conclusions and perspectives will be reported in Section 5.

2. Experimental

2.1. Description of the investigated *PEMFC* stack

The experimented stack is a 12-cell *PEMFC* designed to operate in *μCHP* mode. The stack is fed by air at cathode, and at anode by a fuel mixture (75 % of hydrogen - H_2 and 25 % of carbone dioxide - CO_2) simulating a reformat of natural gas. The *FC* is marketed by Riesaer Brennstoffzellentechnik *GmbH* and Inhouse Engineering *GmbH,* Germany. It is made of graphite gas distributor plates. Its size is 270 mm x 170 mm x 270 mm. The electrode active surface is 196 cm^2. The stack operates with a nominal current of 80 A. A summary of the *FC* nominal operating parameters, and including other main characteristics, is given in Table 1. On the tested *FC*, two coupling-blocks are embedded at stack inlets and outlets in order to integrate (Fig. 2):

- gas pressure and temperature sensors at stack inlets and outlets,
- humidity sensors at stack inlets,
- pressure and temperature sensors on the water-cooling circuit.

Table 1. Summary of the experimented stack characteristics and reference operating parameters.

PEMFC application field	*μCHP*
Manufacturer	*Inhouse Engineering GmbH - Germany*
Number of cells	12
Active surface of electrode	196 cm^2
Gas distributor plates	Graphite
Fuel used during testing	75% H_2 + 25% CO_2 (in Volume)
Coolant flow (deionized water)	3 l/min
Anode stoichiometry (75% H_2 and 25 % CO_2)	1.3
Cathode stoichiometry (air)	2
Relative pressure for H_2 inlet	11 kPa
Relative pressure for air inlet	5 kPa
Max. anode - cathode pressure gap	20 kPa
FC temperature (at outlet of the cooling circuit)	70°C
Anode Relative Humidity (80°C)	50%
Cathode Relative Humidity (80°C)	50%
Load current	80 A

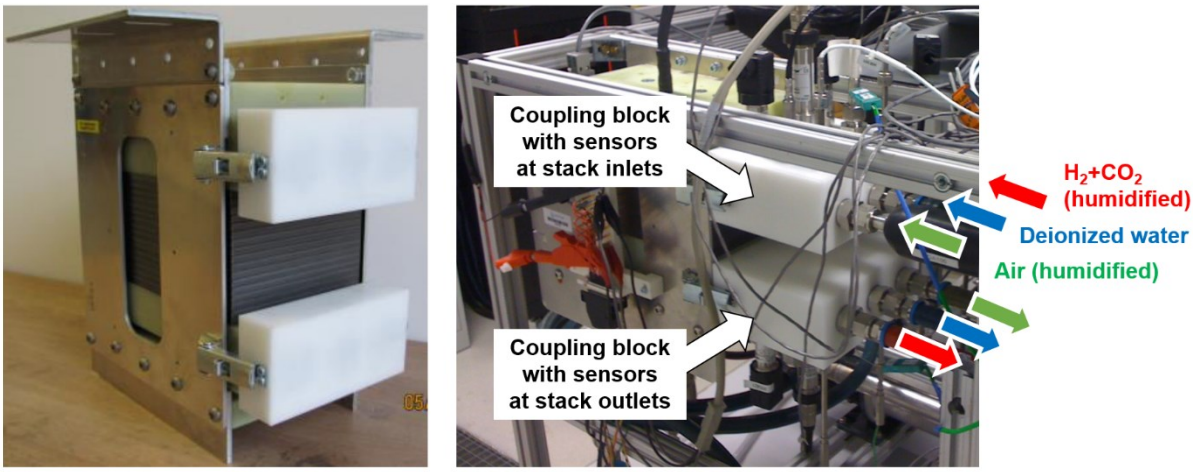

Fig. 2. Pictures of the investigated *PEMFC* stack designed for *μCHP* operation mode. Left: stack only. Right: stack instrumented and integrated in the testbench.

2.2. Testbench architecture description

The above-described FC was experimented with a testbench developed in the *FC* platform of Belfort, France. It includes mainly (Fig. 3):

- a complete gas conditioning sub-system including gas humidifiers at anode and cathode,

- a teststand section dedicated to the control of the temperature inside the stack and including the *FC* primary water circuit.
- an electric / electronic management sub-system,
- an electronic load (TDI Dynaload RBL488 SERIES 800 W) to impose the current in the *FC* stack.

The monitoring and the control of the *FC* testbench parameters are done with National Instruments materials and using a dedicated software. A friendly Human-Machine Interface (*HMI*) was also developed in-lab using Labview™.

The *FC* stack voltage terminals are connected to a SCXI-1313 high-voltage attenuator terminal block used in combination with a SCXI-1125 isolated analog input conditioning module. This latter analog input is then numerised by a 12-bit analog I/O PXI-6070E. The final resolution obtained for the *FC* voltage record is close to 7 mV.

The testbench is also coupled with an electrochemical test station from Materials Mates (*MM*2) Italia. This material allows to record impedance spectra of the complete *FC* stack simultaneously with spectra of the individual cells.

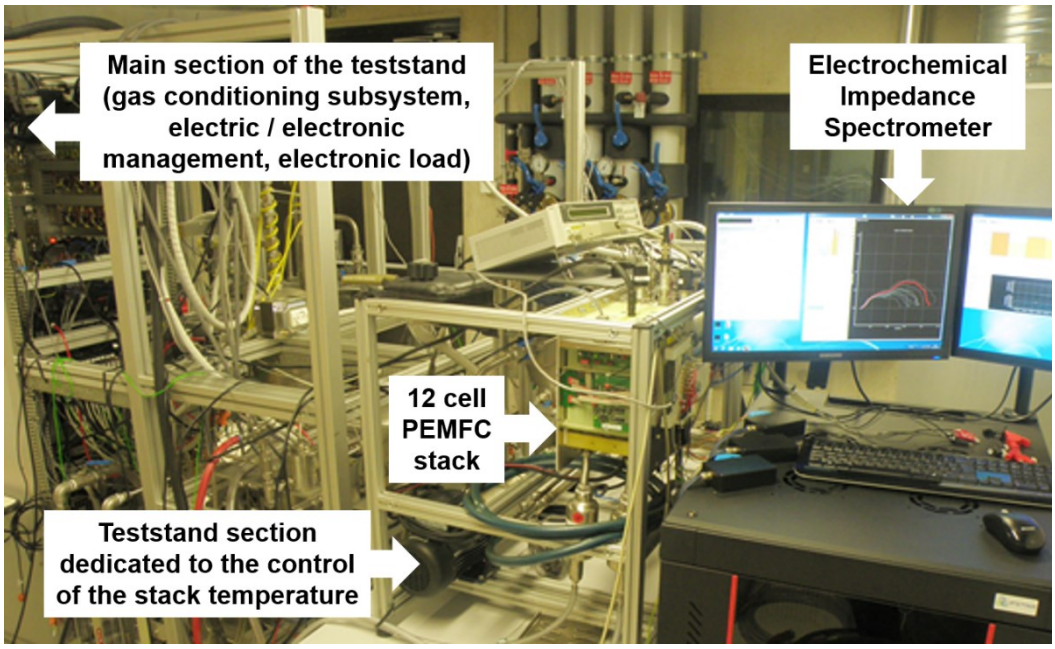

Fig.3. Picture of the PEMFC teststand with its different sub-systems.

2.3. *PEMFC* test protocol

When any *FC* operational parameters are incorrectly deflected from their nominal (or normal) values and are not adjusted, the stack performance may be severely affected. The damages could be irreversible and even dramatically reduce the *FC* lifetime. Therefore, the purpose of the experimental protocol was to introduce different controlled health states into the *PEMFC* stack by configuring various operating

parameters. Two *PEMFC* health states were set: no stack failure state (the *FC* is operating under normal parameters) and with stack failure state (the *FC* is operating under abnormal / severe parameters).

Several scenarios of *FC* system failure were associated to different settings of physical parameters applied through the control-command interface of the testbench, namely: cathode stoichiometry rate (λc), cooling circuit temperature (T), and Relative Humidity (RH) level. The set of the PEFMC tests both performed in the reference conditions and using the degrading operating parameters is reported in Table 2. These tests duplicate various states and faults (actually relative slight deviations from the reference conditions), which are representative for the application environment of μCHP appliance. The following additional explanations are given about the various operating scenarios considered in the experimental campaign.

- The reference Operating Condition (*OC1*) correspond to the "no fault case" (air flow rate of 31.8 Nl/min, fuel flow rate of 8.7 Nl/min, and dew point temperatures of 60°C). Note that the operating conditions selected in this study as the reference ones do not necessarily induce optimal performances of the *FC* stack.
- The failure of the air supply system is reflected by an abnormal value of the λc parameter. This dysfunction may be related with a bad adjustment of the compressor speed (i.e. problem with the control of the compressor), with a mechanical failure in the compressor head, or with a possible leakage in the air section upstream of the stack. The failure of the air supply section may have different consequences for the *FC* stack behavior: more or less pronounced cases of oxidant starvation, Membrane Electrode Assembly - *MEA* drying for too high cathode stoichiometry values, flow-field channels obstruction by liquid water for too low cathode stoichiometry rates. The default related with a higher cathode stoichiometry factor is obtained with λc = 2.6 (Operating Condition *OC2*: O_2 over-supply, with an air flow rate of 41.5 Nl/min). The default related with a lower cathode stoichiometry factor is obtained with λc = 1.6 (Operating Condition *OC3*: O_2 under-supply (slight starvation), with an air flow rate of 25.8 Nl/min instead of 31.8 Nl/min).
- The failure of the cooling circuit is featured by the stack temperature (T). This failure can be caused by a slower velocity of the pump in the cooling circuit, a damage on the primary or secondary heat exchanger, or by any control-command problem. The defaults of the cooling circuit temperature are induced with T = 65°C (Operating Condition *OC4*: temperature lower than the reference value) or with T = 72°C (Operating Condition *OC5*: temperature higher than the reference level).
- The failure of the gas humidification section leads to the flooding or the drying of the *PEMFC* core (*MEA*). This abnormal *FC SoH* can be detected by the measurement of the high frequency (close to 1 kHz) cell resistance that leads to an estimation of the amount of water in the membrane. This failure scenario is featured by the Relative Humidity (RH) parameter (or possibly by the dew point temperature in the humidification section of the system). This failure associated to the bad humidification of the gases can be related with a dysfunction of the humidification unit. The default of the Relative Humidity

is obtained with *RH* = 54 % (Operating Condition *OC6*: towards a stack flooding, dew point temperature of 65°C instead of 60°C as in the reference case).

Table 2. The Operating Conditions (*OC1*, … , *OC6*) induced during the experimental campaign conducted with the investigated *PEMFC*. The parameter values in bold and underlined correspond to the introduced faults.

	OC1	***OC2***	***OC3***	***OC4***	***OC5***	***OC6***
λc	2	**2.6**	**1.6**	2	2	2
T (°C)	70	70	70	**65**	**72**	70
RH (%)	50	50	50	50	50	**54**

The experiments carried out are used to create an extensive database, which includes many physical signals measured from the stack and testbench ancillaries such as gas pressures, flows, temperatures, humidity rates, power, individual cells voltages… In general, all the data are acquired with a sampling frequency of 3 Hz. However, the voltage stack signal considered as the useful signal for our diagnosis algorithms is recorded using LabView with a higher frequency (f_s) of 3 kHz, both for nominal and faulty operating conditions. Note that the selected frequency value is close to the one chosen by Maiza et al. in [18] to study the *FC* electrochemical noise (data acquisition at 2 kHz), but slightly lower than the sample rate of 10 kHz used in the work of Rubio et al. [30]. Some examples of the acquired stack voltage signals are shown in Fig. 4. The voltage analysis is made in the Matlab™ environment.

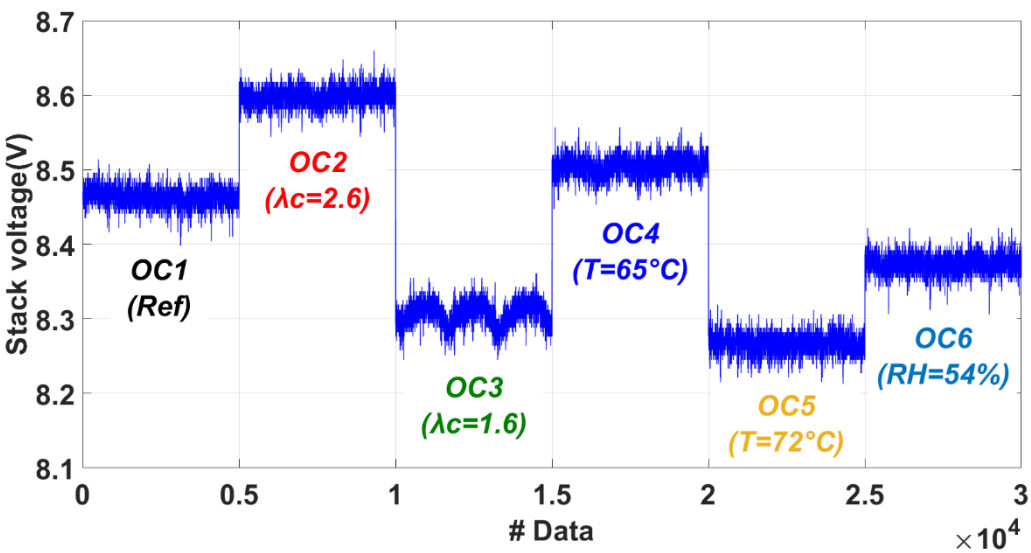

Fig. 4. Typical stack voltage signals of the studied *PEMFC* operated in normal and abnormal Operating Conditions (*OC1*, … , *OC6*), with f_s = 3 kHz.

In addition, Electrochemical Impedance Spectra (*EIS*) for the individual cells and for the stack are recorded in the 0.1 Hz to 10 kHz frequency range. The *EIS* measurements are performed with an electrochemical impedance spectrometer shown in Fig. 3. During the *EIS* tests, the instrument operates in galvanostatic mode (the load current is imposed while the stack and cell voltages are measured). According to the *EIS* procedure, the *AC* sine wave is generated and imposed over the *DC* excitation. The *AC* sine wave magnitude is equal to ±10% of the *DC* load value. Modulated frequencies between 10 kHz and 0.1 Hz are applied and 10 points / decade are selected. This leads to 50 measurement points for a complete spectrum (i.e. a display of the stack impedance *Z* using a Nyquist plot, for the frequency range considered). The record duration for a spectrum equals to 8 min approximately.

3. How to build the low- and high-frequency *VSS* signatures?

A signal is the physical representation of information, which is transmitted from its source to the user. Therefore, the stack voltage signal can be considered as an informative signal, which contains relevant information on the *FC SoH*. We consider that any change in the operating conditions of the *PEMFC* affects the amplitude of the voltage signal produced and its morphology (Fig. 4). A fine analysis of this signal using adequate tools allows the extraction of relevant features to perform the *PEMFC SoH* monitoring. This was already shown by the results of singularity analyses applied to *FC* voltage signals obtained in a previous study with a *PEMFC* dedicated to a **transport application**, depicted in [20-25]. In these previous works, the analyzed voltage signals were acquired at a frequency of **11Hz.** Thus, the voltage signals obtained contained information describing the low frequency (1Hz - 5.5Hz) dynamics of the *PEMFC* physical phenomena, such as mass transport phenomena.

In the present work, the investigated voltage signal is recorded at a higher frequency of **3 kHz** from a *PEMFC* designed for a ***μCHP* application**. In this case, it is therefore possible to access to a wider range of frequency dynamics related with the physical phenomena occurring in this *PEMFC*. For example, the high frequency resistance (or internal resistance) related with the *FC* membrane *SoH* can typically be measured at a frequency close to 1 kHz (usually between 1 kHz and 10 kHz) [26, 30, 31].

In this work and in a first approach, we intend to focus on high and low frequency electrochemical phenomena (i.e. linked with the FC membrane *SoH* on the one hand, and with mass transports on the other hand) and we aim to distinguish FC operating states linked with these two distinct frequency ranges. At this stage of our work, the study of intermediate frequency phenomena (with a coupling of charge transfers and mass transports) remains an issue for future researches.

As mentioned in the introduction of the article, the first step of the diagnosis strategy (Fig. 1) deals with the voltage signal deep analysis and it contains two analysis blocks (Block 1.1: signal filtering, and Block 1.2: singularity computation). These blocks are described hereafter.

- ***Block* 1.1 → *High frequency voltage signal filtering.*** The application of a pre-processing operation based on the filtering of the original high frequency voltage signal is a natural option to separate the high frequency information (frequency range above 1 kHz, a value related with the membrane resistance value and its water content) from the low frequency one, enclosed in the signal (frequency range below 1 Hz, a value linked with mass transport phenomena). This information reflects the high and low frequency dynamics of the *FC* physical phenomena. The signal filtering is realized using a *Butterworth filter*, one of the filters commonly used in filtering processes of digital signals, which is easy to synthetize [32, 33].

The original voltage signal is filtered twice. First, the Butterworth high-pass filtering, which allows to pass high frequency and to stop low frequency components, is applied on the original signal. The original signal is filtered a second time with the Butterworth low-pass filter to pass the low frequency components only.

As a short description of the filter used, a low-pass analogical Butterworth filter, of *N* positive integer order (in our case, *N* = 1), obeys the following function in the frequency domain:

$$|R(j\omega)|^2 = \frac{1}{1+\left(\frac{\omega}{\omega_c}\right)^{2N}} \quad (1)$$

Where:

$|R(j\omega)|^2$ is the square magnitude of the frequency response of the filter,

$\omega = 2\pi f$ is the angular frequency (rad / s), with *f* the frequency (Hz),

ω_c is the filter cutoff frequency (rad / s),

and $j^2 = -1$.

This low-pass filter is used as a prototype for the construction of other filter's class by mathematical methods of frequency transformation [34].

The results obtained with the Butterworth high-pass filtering (cut-off frequency of 1 kHz), applied to the original voltage signal of Fig. 5 (a), are shown in Fig. 5 (c1). The low frequency signal, resulting from the Butterworth low-pass filtering with a cut-off frequency of 1 Hz, is shown in Fig. 5 (c2).

The frequency responses of the two applied Butterworth filter classes are plotted in Fig. 5 (b1 and b2).

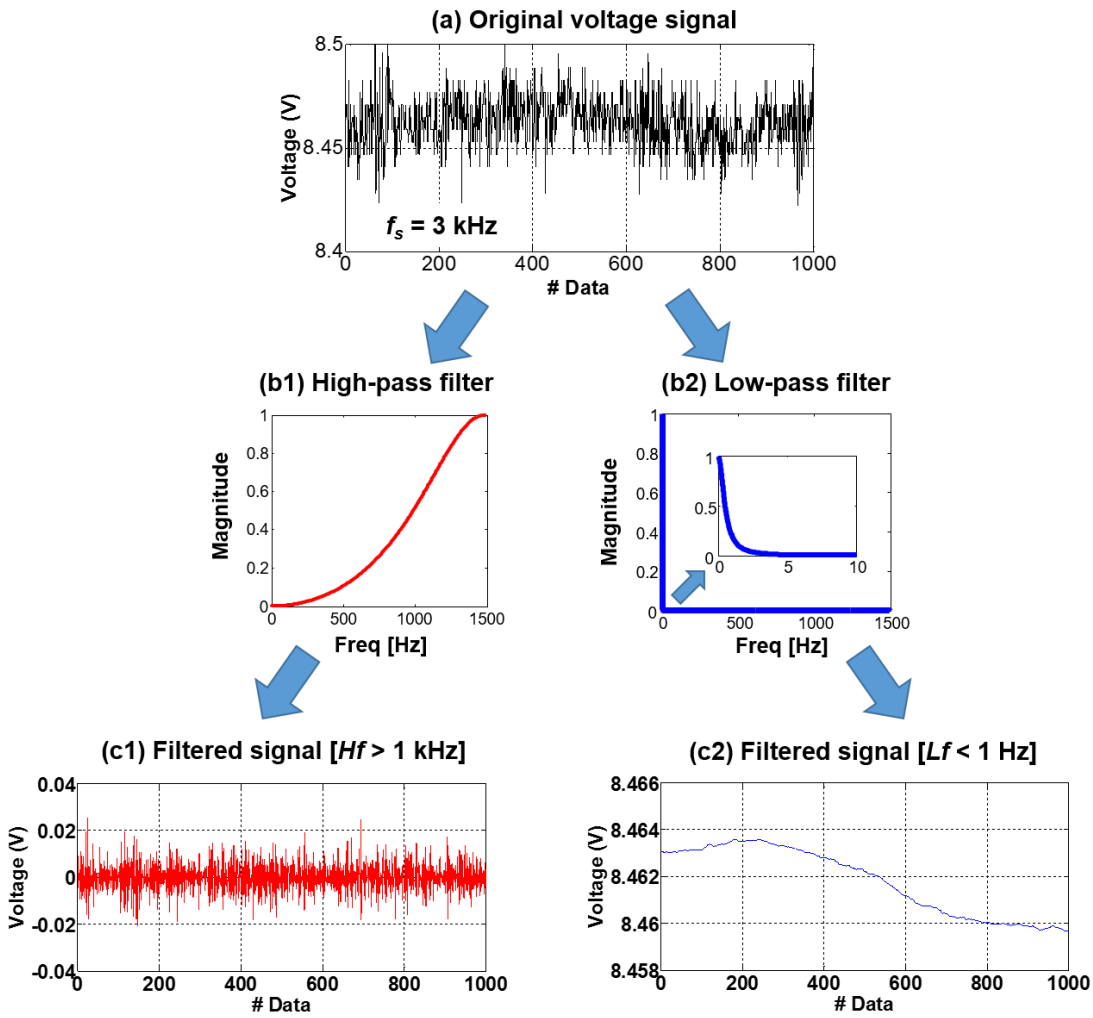

Fig. 5. Stack voltage signal filtering process using two classes of *Butterworth filter*: a) original voltage signal, b1) high-pass filter frequency response and c1) the corresponding filtered voltage signal, b2) low-pass filter frequency response and c2) the resulting filtered signal.

- ***Block* 1.2 → *Singularity Spectrum (SS) computation.*** Scale invariance is a widely used concept to analyze real-world data from many different applications and singularity analysis has become a promising corresponding signal-processing tool [35-37]. It allows the characterization of data by describing globally and geometrically the fluctuations of local regularity, usually measured by means of the Hölder exponent.

The singularity analysis, also named "multifractal analysis", describes the time (t) based fluctuations of the signal given by a function *X(t)*. This is achieved by comparing the local variations of *X(t)* around fixed time position t_0, against a local power law behavior: $X(t_0)$ belongs to $C^{\alpha}(t_0)$ with $\alpha \geq 0$ if there are a positive constant C and a polynomial P, satisfying $\deg(P) < \alpha$, such that:

$$\left|X(t) - P_{t_0}(t)\right| \leq C|t - t_0|^{\alpha} \quad (2)$$

The Hölder exponent is defined as the largest α such as: $h(t_0) = sup\{\alpha: X \in C^{\alpha}(t_0)\}$.

The singularity strength regarding the variability of the regularity of *X(t)* vs. *t* is usually described through the so-called singularity spectrum. Building a singularity spectrum consists in associating to each Hölder exponent *h* the Hausdorff dimension *D(h)* of the sets of points which exhibit the same value of *h*. This can be achieved using the Wavelet Leader Multifractal Formalism [38, 39]. Detailed descriptions of the theoretical and practical relevance and benefits of the use of wavelet leaders for singularity analysis are depicted in [20-25, 37-39]. In Fig. 6, an example of singularity spectrum obtained from a voltage signal, named Voltage Singularity Spectrum (*VSS*), is shown and some singularity features are highlighted. The singularity feature h_0 reflects the dominant singularity strength in the signal, which means a singularity value that is the most prominent in the signal support. The multifractal behavior of the signal, exhibited by the shape of the *VSS* in the form of a concave arc, reveals the existence of a certain order in its structure, which obeys a scale invariance property.

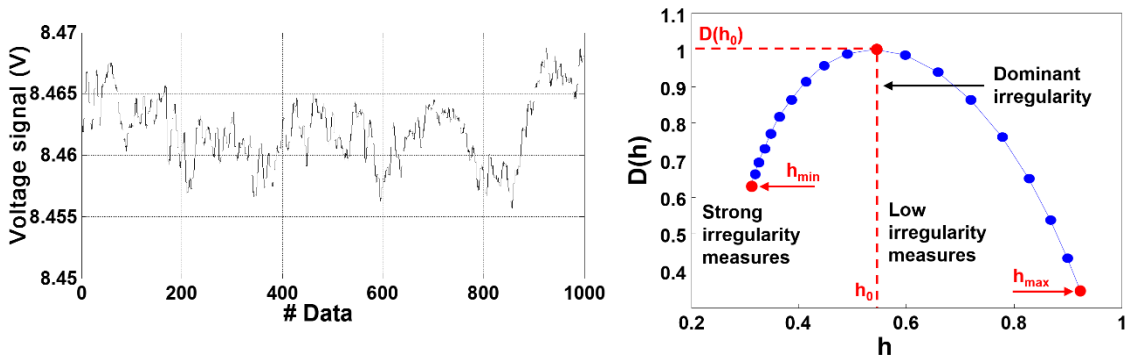

Fig.6. Typical curves of the stack voltage signal (left) and its corresponding *VSS* (right).

In this study, the Wavelet Leader Multifractal Analysis (*WLMA*) is implemented on both the filtered *Hf* and *Lf* voltage signals. The V*SS* computation is performed for normal and abnormal *PEMFC* operating conditions. To show the interest of the pre-processing filtering operation, the *VSS* is computed from the raw voltage signal of the stack (original signal without the filtering operation). The *VSS* obtained from the voltage signals without the filtering operation in one hand, and from the *Hf* and the *Lf* filtered signals in other hand, are exhibited respectively in Fig. 7 a) and 7 b). The *VSS* are computed for different operating conditions listed in Table 2.

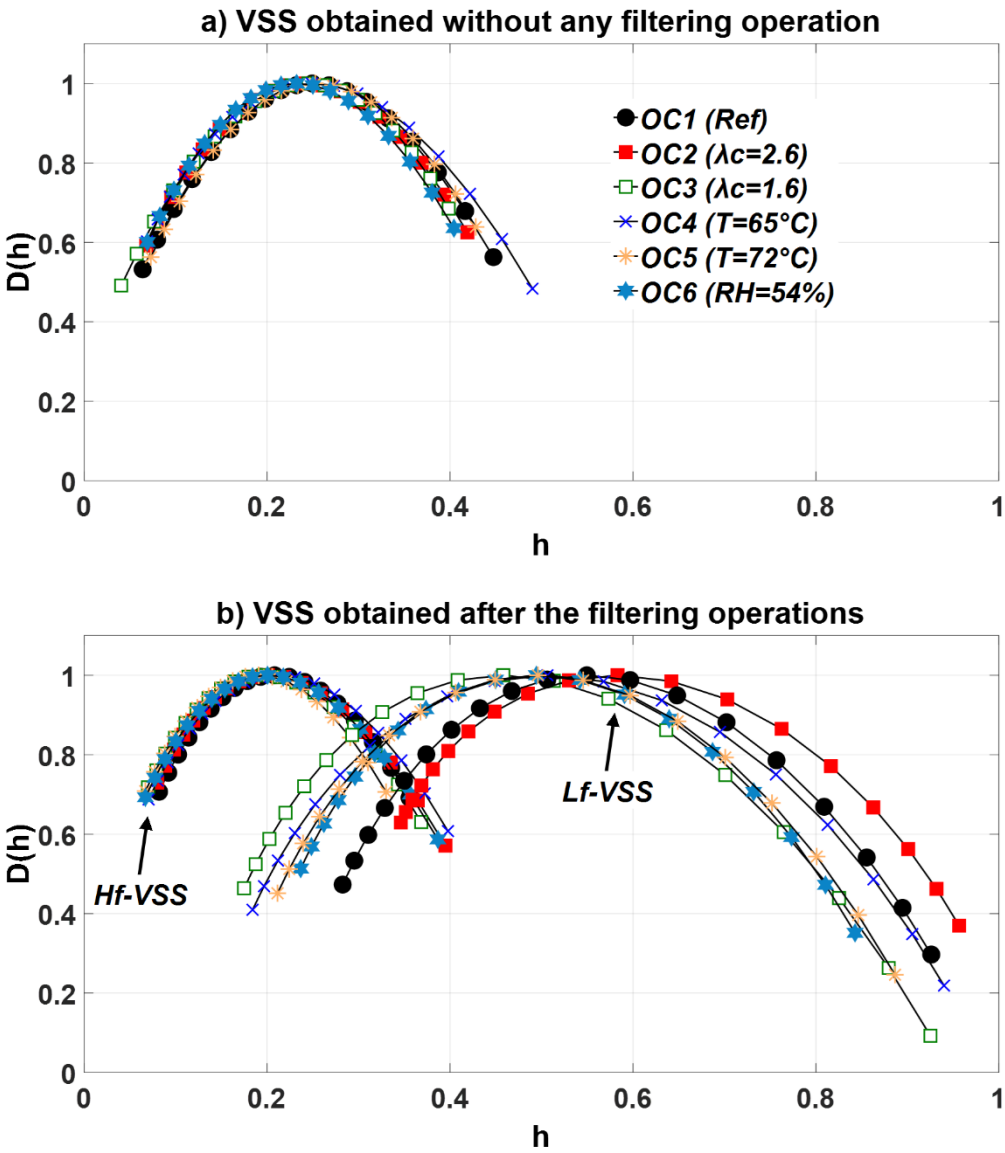

Fig.7. Results of the *VSS* obtained for normal (*Ref*) and abnormal Operating Conditions (*OC*), for: a) raw voltage signals with *fs* =3 kHz, b) high and low filtered voltage signals (respectively *Hf-VSS* and *Lf-VSS*).

As shown in Fig. 7 (a), we obtain one location for the *VSS* computed from the non-filtered voltage signals, with Hölder exponent '*h*' values belonging to the interval [0, 0.5], with the average of h = 0.20±0.08. The *VSS* resulting from the *Hf* and the *Lf* filtered voltage signals (Fig. 7 (b)) are located at two separate intervals on the *h* axis. Indeed, the *Hf-VSS* are shifted to the left; the interval of the *h* values is [0, 0.4] and the average of h = 0.20±0.09. In this case, the voltage signal encloses strong irregularity strengths. The *Lf-VSS* are shifted to the right, with *h* values in the range of [0.2, 1], with the average of h = 0.47±0.25 because of the low irregularity points incorporated in the *Lf* filtered signals.

However, if we consider the *VSS* obtained from the non-filtered signals and those obtained from the *Hf* filtered signals, we can observe that both the *VSS* locations and the average of *h* are relatively close.

In other terms, the *VSS* computed on the non-filtered signals do not allow the discrimination between the high and low frequency dynamics of the *FC* physical phenomena and only *Hf-VSS* are highlighted. This can be explained by the fact that the high frequency information seems to be the most prominent component in the non-filtered signal and the low frequency information is hidden. Hence, the interest of the signal filtering pre-processing operation to access to a wide range of frequency components for the voltage signal studied.

4. *VSS* - *EIS* comparisons and use of pattern parameters for diagnostic purpose

For a further analysis, the results of the *VSS* are compared with the *EIS* in Fig. 8. Both analysis tools are applied for the same Operating Conditions (*OC*) of the studied *FC* (1 normal and 5 abnormal *OC*).

In this section, the real parts *Re(Z)* in the Nyquist diagram corresponding respectively to the high- and low-frequency resistances (*Hf-Re(Z)* and *Lf-Re(Z)*) are extracted from the *EIS*, at the two frequency intervals [1 - 1.5] kHz and [0.1 - 1] Hz (Fig. 8). These values are compared to the singularity feature h_0, which reveals the dominant singularity strength or the prominent irregularity degree in the signal and can be measured on the *Hf-VSS* and *Lf-VSS*. The resulting values of *Hf-Re(Z)*, *Lf-Re(Z)*, and h_0 are reported in Fig. 8 in the form of bar diagrams for the 6 studied *OC*.

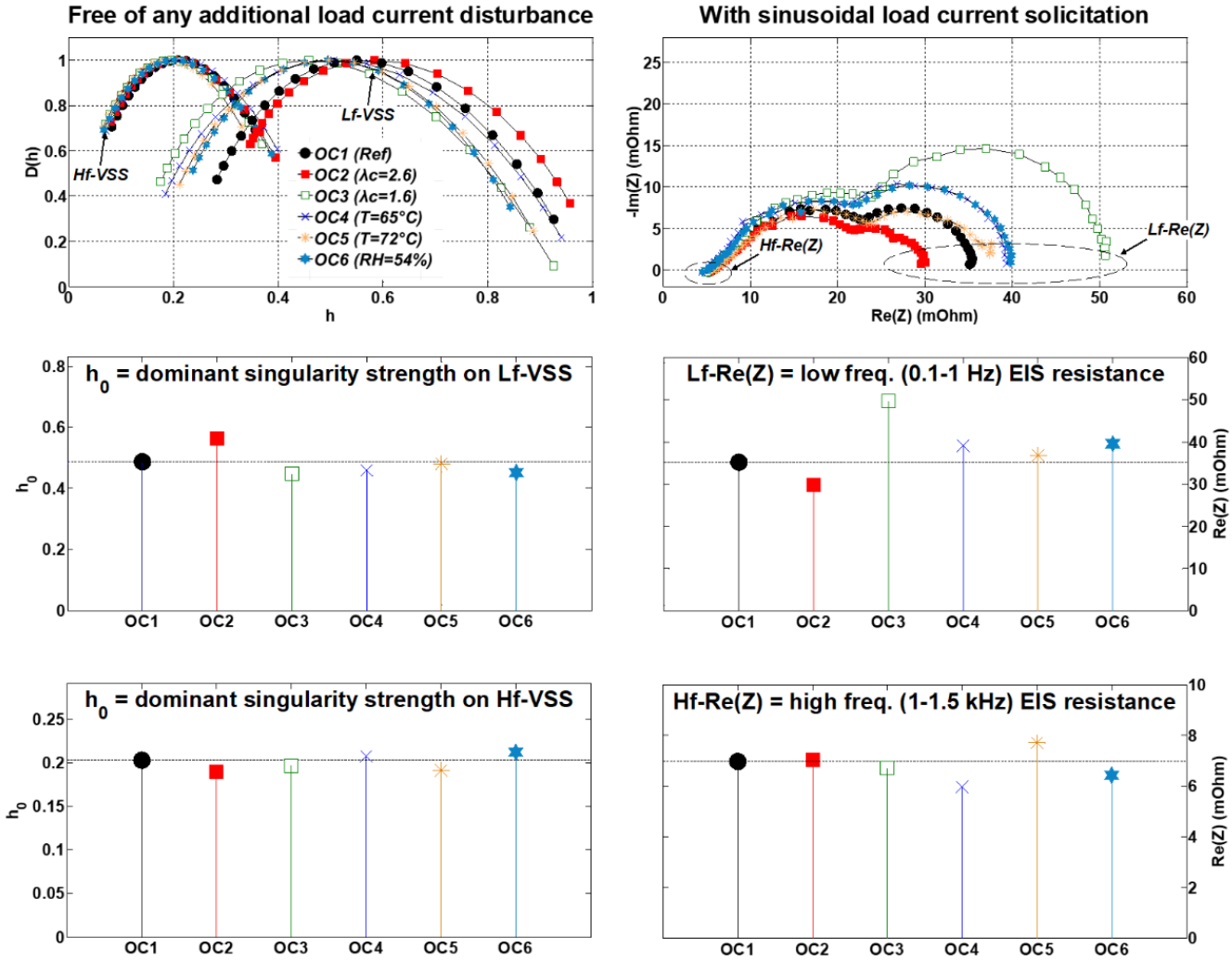

Fig. 8. Comparative study between *VSS* and *EIS* analysis tools.

Up: *VSS* results vs. *EIS* ones are represented for 6 *OC* of the *FC* (1 normal and 5 abnormal *OC*).

Middle: Bar diagram plots given for dominant singularity strengths from *Lf-VSS*, compared to low frequency resistances *Lf-Re(Z)* from *EIS* (*Lf* = [0.1 - 1] Hz).

Below: Bar diagram plots for dominant singularity strengths from *Hf-VSS*, compared to high frequency resistances *Hf-Re(Z)* from *EIS* (*Hf* = [1 - 1.5] kHz). Horizontal dashed lines (--) of the bar diagrams highlight both dominant singularity strength and resistance values resulting from the *FC* normal *OC*.

The results obtained for the two frequency intervals are analyzed and discussed below.

- *Low frequency interval results* (see. Fig. 8 (middle)): In this case, the *FC* normal operating conditions OC_1 produce a voltage signal that contains irregular points with a dominant singularity strength $h_0 = 0.48$ corresponding to a low frequency resistance *Lf-Re(Z)* = 35 mΩ. For the abnormal *OC* (*OC*2, *OC*3, …, *OC*6), we can observe that the magnitude of the stems representing the dominant singularity strengths h_0 follows a reverse tendency compared to those indicating the low frequency

resistances (viz. related with the mass transport resistance and the polarization resistance *Lf-Re(Z)*). In other words, a high magnitude of the stems representing *Re(Z)* corresponds to a low magnitude of the stems describing h_0. For a low value of *Re(Z)*, a high value of h_0 is exhibited. As an example, let us consider two abnormal *FC* states of health (*SoH*). The first state is the abnormal operating conditions *OC*3 (viz. the oxygen starvation, with λc = 1.6). The low frequency resistance *Lf-Re(Z)* estimated for these conditions equals 50 mΩ. This value is greater than the one computed for the air oversupply abnormal state of the *FC* operated under *OC*2 (with λc = 2.6), which equals 30 mΩ. On the contrary, the value of the *OC*3 singularity feature h_0 (= 0.45) is lower than h_0 (= 0.56) for *OC*2.

- *High frequency interval results* (see. Fig. 8 (down)): The *FC* operated under *OC*1 produces a very rough voltage signal, with h_0 = 0.2 corresponding to a high frequency resistance *Hf-Re(Z)* = 7 mΩ. For other *OC* situations, an inverse trend between the bar diagrams related to *Hf-Re(Z)* (internal resistance of the *FC*) and the singularity feature h_0 estimated from the *Hf-VSS* can possibly be noticed. However, the values of the two parameters do not exhibit large changes for the different *OC*. This can be explained by the fact that the *FC* membrane *SoH* is not affected by the small changes in abnormal *OC*.

After a finer analysis of these results, we conclude that:

- A high value of h_0 reveals a regular voltage signal, for which low resistance values of *Lf-Re(Z)* and *Hf-Re(Z)* were measured using the *EIS*.
- A low value of h_0 reveals a strong irregular voltage signal, for which high resistance values of *Lf-Re(Z)* and *Hf-Re(Z)* were measured in the *EIS*.

At this stage, the h_0 parameter can already be considered as a good indicator of the *FC SoH*. In the following part, we intend to provide a more detailed analysis and comparison of the *VSS* and *EIS* results obtained, for the following purposes:

- to better highlight the links between the *Lf-*h_0 and *Lf-Re(Z)* parameters on the one hand, between the *Hf-*h_0 and *Hf-Re(Z)* parameters on the other hand,
- with a view to diagnosis, to show how the *Lf-* h_0 and *Hf-* h_0 parameters can possibly be used to characterize some of the *FC SoH*, as it can usually be done using well-suited *EIS* parameters [27].

To reach these aims, the dominant singularity strengths h_0 computed for the 6 Operating Conditions (*OC1*, …, *OC*6) are plotted as a function of the corresponding impedance real parts *Re(Z)* with the aim of looking for any possible relations between the two types of parameters. The plot and analysis are done both at low frequency (plot of *Lf-*h_0 vs. *Lf-Re(Z)*, Fig. 9) and high frequency (plot of *Hf-*h_0 vs. *Hf-Re(Z)*, Fig. 10).

Analysis of the *Lf-*h_0 vs. *Lf-Re(Z)* plot (Fig. 9):

The graph (Fig. 9 a) or b)) indicates that higher values of h_0 are obtained for lower resistance values of *Lf-Re(Z)*. *Lf-*h_0 appears as a monotonous decreasing function of *Lf-Re(Z)*. A basic linear regression

model can be computed from the six value pairs; this linear model already leads to a good coefficient of determination (*R-squared*) equal to 0.669 (*adjusted R-Squared* of 0.586). For the record, the *R-squared* coefficient indicates the proportionate amount of variation in the response variable Y explained by the independent variables X in the linear regression model. The larger the *R-squared* is, the more variability is explained by the linear regression model. It would obviously be possible to propose a higher order model for the relationship between $Lf\text{-}h_0$ and *Lf-Re(Z)*. However, at his stage of our work, this model would not have any particular physical significance. We therefore prefer to show by other means how the $Lf\text{-}h_0$ feature could be used to establish the *FC SoH* diagnosis, as it is often done with the *Lf-Re(Z)* parameter. Indeed, the variation of the *Lf-Re(Z)* parameter can be exploited to detect various *FC* operating conditions linked with different gas supplies. For instance, on the graph $Lf\text{-}h_0$ vs. *Lf-Re(Z)*, we observe that a high cathode stoichiometry rate applied for *OC2* (λc = 2.6) leads to a reduction of the *Lf-Re(Z)* value (case of a higher, better oxygen diffusion). In contrast, we can also observe that a low cathode stoichiometry rate applied for *OC3* (λc = 1.6) induces an increase of the *Lf-Re(Z)* value (case of a lower oxygen diffusion). The operating conditions *OC1*, *OC5*, *OC4*, and *OC6* lead to intermediate *Lf-Re(Z)* values which cannot really be related with better or poorer oxygen diffusion. In order to highlight these three groups of *Lf-Re(Z)* values in a more formal framwork, we propose to apply a simple data clustering process to generate the three clusters (with the labels: "better diffusion", "normal", "poorer diffusion") from the 6 *Lf-Re(Z)* values. The clustering is achieved using the *kmeans* method in the Matlab™ environment and the result is displayed in the graph $Lf\text{-}h_0$ vs. *Lf-Re(Z)* (Fig. 9 a)). The same clustering process can be applied to the six *OC*, described by the six related $Lf\text{-}h_0$ values (Fig. 9 b)). The resulting clustering is slightly different from the previous one. Again, a cluster is associated to *OC2* (λc = 2.6) with $Lf\text{-}h_0$ = 0.56, corresponding to the "better diffusion" case. Another cluster (the "normal" one) consists of *OC4* and *OC5*, while a third cluster including *OC4*, *OC6*, and *OC3*, shows the lowest $Lf\text{-}h_0$ values and is related with the "poorer diffusion" case. When comparing the clustering results obtained from the *Lf-Re(Z)* values on the one hand and from the $Lf\text{-}h_0$ values on the other hand, it can be observed that there is a kind of confusion or uncertainty for *OC4* and *OC6*, which can be considered as belonging either to the "normal case" cluster or to the "poorer diffusion" cluster (in fact, they correspond to intermediate cases between the *OC1-OC5* group, and *OC3*). The other *OC* are classified in the same way, whatever the parameter considered (*Lf-Re(Z)* or $Lf\text{-}h_0$). At this late stage, our study indicates that the $Lf\text{-}h_0$ feature can be considered to diagnose the impact of λc on the diffusion in the *FC*, at least for the two "extreme" cases (λc = 2.6 and λc = 1.6), and in the same way as what can be done from the *Lf-Re(Z)* parameter measured through *EIS*.

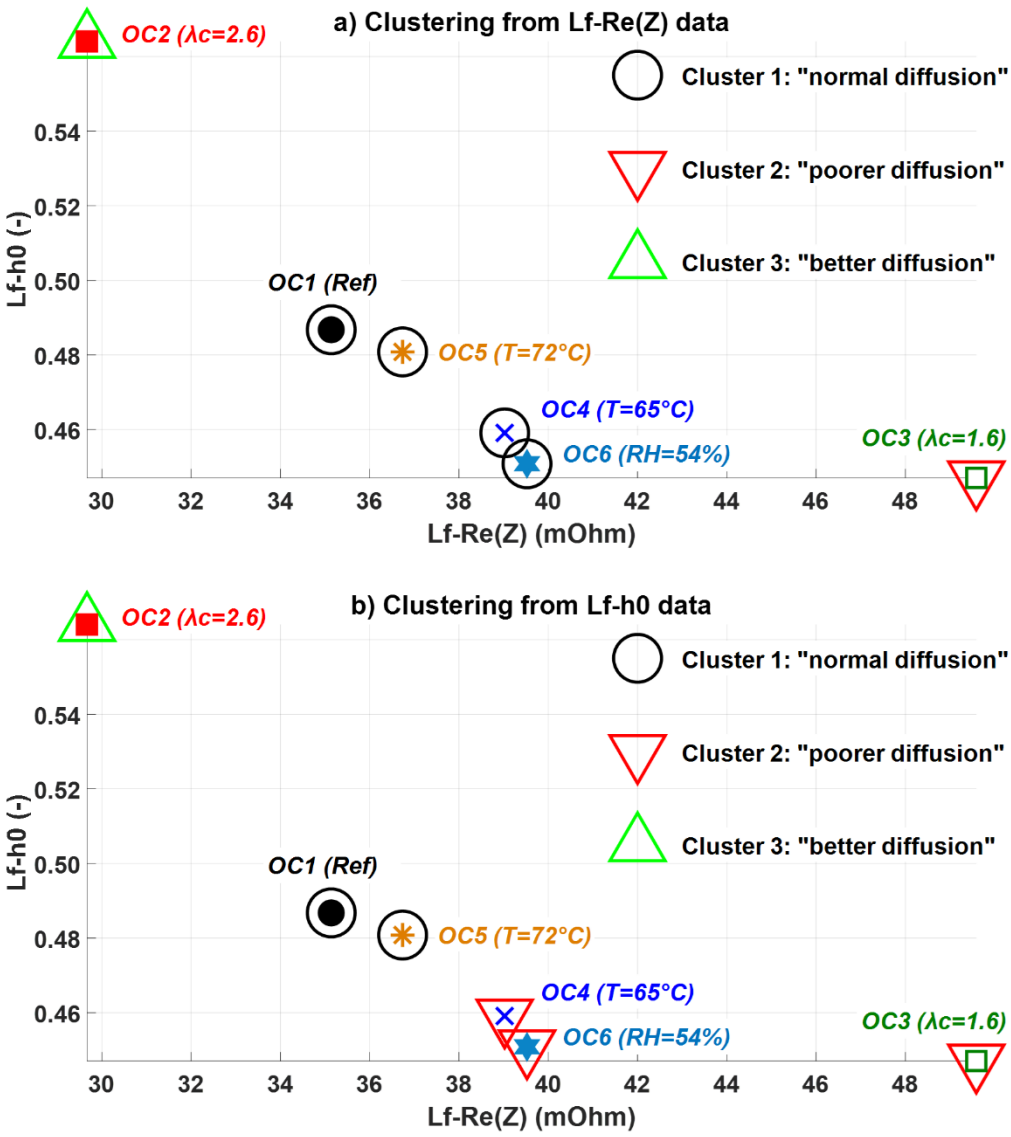

Fig. 9. For the 6 Operating Conditions (*OC*), plot of *Lf-h₀*, the dominant singularity strength measured on the *Lf-VSS*, as a function of *Lf-Re(Z)*, the resistance intercepted on the *EIS* x-axis at low frequency.

a) Up: clustering of the *OC* done from the *Lf-Re(Z)* data.

b) Down: clustering of the *OC* done from the *Lf-h₀* data.

Analysis of the *Hf-h₀* vs. *Hf-Re(Z)* plot (Fig. 10):

Overall, the graph (Fig. 10 a) or b)) shows that higher values of *Hf-h₀* are obtained for lower resistance values of *Hf-Re(Z)*. However, compared to the *Lf-h₀* vs. *Lf-Re(Z)* plot, the trend is not so clear: *Hf-h₀* does not appear as a monotonous decreasing function of *Hf-Re(Z)*. Nevertheless, as we did for the *Lf-h₀* feature, we intend to show how the *Hf-h₀* parameter could be used for the determination of the *FC SoH*, as it is usually done with the *Hf-Re(Z)* parameter. Indeed, the *Hf-Re(Z)* parameter can be monitored to detect various operating conditions linked with different hydration states of the *MEA*. For example, on the *Hf-h₀* vs. *Hf-Re(Z)* plot, we observe that a lower *FC* operating temperature set for *OC4* ($T = 65°C$)

and a higher gas hygrometry rate applied for *OC6* (*RH* = 54%) lead to a reduction of the *Hf-Re(Z)* value (case of a better *MEA* hydration and decrease of the *HF* membrane resistance). On the contrary, we can also observe that a temperature higher than the reference one (for *OC5* with *T* = 72°C) induces an increase of the *Hf-Re(Z)* value (case of lower MEA hydration, drying of the membranes). The operating conditions *OC3*, *OC1*, and *OC2* lead to intermediate *Hf-Re(Z)* values which cannot be related with better or lower *MEA* hydration. In order to highlight these three groups of *Hf-Re(Z)* values, and in a similar way to what was done for *Lf-Re(Z)*, we apply the *kmeans* data clustering process to generate three clusters (with the labels: "better *MEA* hydration", "normal *MEA* hydration", "lower *MEA* hydration") from the 6 *Hf-Re(Z)* values. The resulting clustering is displayed in the graph $Hf\text{-}h_0$ vs. *Hf-Re(Z)* (Fig. 10 a)). Then, the same clustering process is applied to the six *OC*, described by the six related $Hf\text{-}h_0$ values (Fig. 10 b)). The clustering results obtained from the *Hf-Re(Z)* values and from the $Hf\text{-}h_0$ values are slightly different. With the $Hf\text{-}h_0$ values, a cluster is associated to *OC4* and *OC6*, corresponding to the "better *MEA* hydration" case. Another cluster ("normal" one) consists of *OC3* and *OC1*, while a third cluster including *OC2* and *OC5* shows the lowest $Lf\text{-}h_0$ values and is related with the "lower *MEA* hydration / drying" case. When comparing the two clustering results obtained from the *Hf-Re(Z)* values and from the $Hf\text{-}h_0$ values, it can be observed that there is a kind of confusion or uncertainty for *OC2* which can be considered as belonging either to the "normal case" cluster or to the "lower *MEA* hydration / drying" cluster. The other *OC* are classified in the same manner, whatever the parameter considered (*Hf-Re(Z)* or $Hf\text{-}h_0$). A this stage, this clustering study indicates that the $Hf\text{-}h_0$ feature could possibly be used to diagnose the *MEA* hydration state, at least for the three "extreme" cases considered (*OC4* and *OC6* on the one hand, *OC5* on the other hand), and similarly to what can be done from the *EIS Hf-Re(Z)* parameter. However, as it was already observed from Fig. 8 and also mentioned at the beginning of this paragraph, the correlation between $Hf\text{-}h_0$ and *Hf-Re(Z)* is not as good as the one established between $Lf\text{-}h_0$ and *Lf-Re(Z)*. Several explanations can be given on this issue. As previously stated, the values of the two parameters could not exhibit large, significant variations during the experiments because only small condition changes were applied for the abnormal *OC*. No pronounced drying or flooding events were induced in the tests, which makes the analysis all the more difficult. Besides, for the high frequency domain considered (at a signal frequency close to 1 kHz), the potential impacts of the *FC* operating environment (i.e. the effects of the auxiliaries, components of the *FC* test bed) on the "free evolution" of the stack voltage are more difficult to understand from a physical point of view, and to measure as well. Further investigations at different levels are needed on this issue. A more accurate measurement and data acquisition chain would be needed, for instance to have the opportunity to highlight and evaluate any possible influence of the load current noise on the *FC* stack morphology.

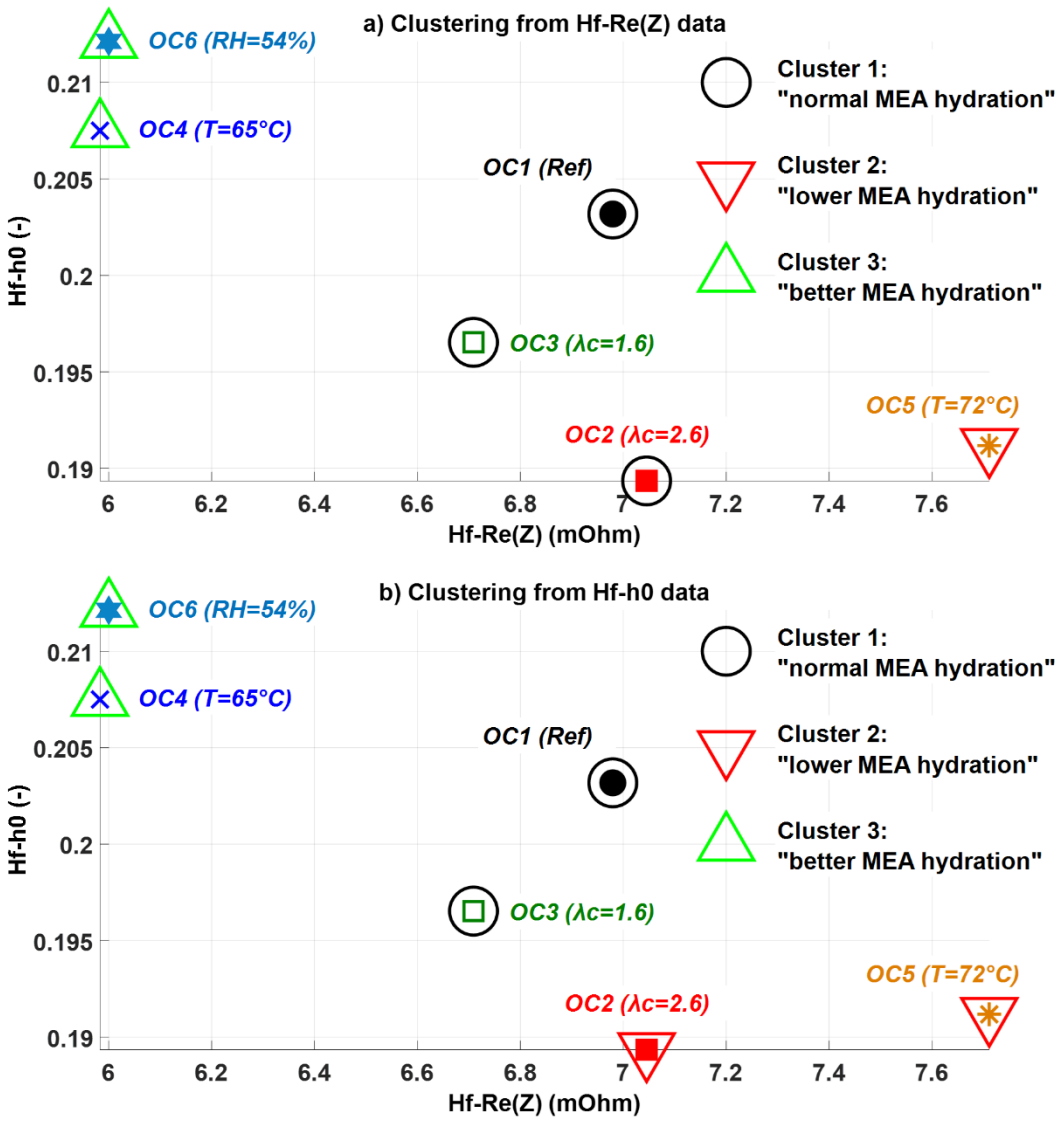

Fig. 10. For the 6 Operating Conditions (*OC*), plot of *Hf-h₀*, the dominant singularity strength measured on the *Hf-VSS*, as a function of *Hf-Re(Z)*, the resistance intercepted on the *EIS* x-axis at high frequency.

a) **Up**: clustering of the *OC* done from the *Hf-Re(Z)* data.

b) **Down**: clustering of the *OC* done from the *Hf-h₀* data.

5. Conclusions

There is currently an urgent need for non-invasive condition monitoring techniques for *FCs* used in commercial applications such as *μCHP* appliances and the idea of processing the natural fluctuations at the stack terminals, without external disturbance, in order to estimate the *FC SoH* is very attractive. In this context, the proposed work offers an alternative signal analysis tool useful for the characterization and *SoH* monitoring of a *PEMFC* fed with a hydrogen-rich mix. The developed tool is based on the measurement of the singularity strength h_0 in a stack voltage signal recorded at a 3 kHz frequency; the selected frequency allows accessing to low and high frequency dynamics (i.e. respectively below 1 Hz and above 1 kHz) linked with physical phenomena occurring in the *FC*. The objective of accessing to these dynamics has to be met with the constraints of implementing a non-invasive and free of any *FC* disturbance analysis tool. In this respect, the Voltage Singularity Spectrum (*VSS*) can be estimated using a non-intrusive manner and without affecting in any way the *FC* operation.

The work is structured in two main phases:

- An experimental phase: a *PEMFC* dedicated to a *μCHP* application is operated using a fuel mixture with 75% of H_2 and 25% of CO_2 under normal and abnormal Operating Conditions (*OC*).
- A data analysis phase: this objective is achieved by the thorough analysis of the collected data enabled by the powerful *WLMA*. The latter is adopted to access to the latent information enclosed in the high frequency recorded stack voltage signal. This information is extracted from low and high frequency filtered signals. Then, two groups of *VSS* are computed for the two frequency ranges (*Lf-VSS* and *Hf-VSS*) and their dominant singularity strengths ($Lf\text{-}h_0$ and $Hf\text{-}h_0$) are extracted.

The comparison of the *VSS* and *EIS* signatures obtained for the 6 *OC* shows the usefulness of the proposed *SoH* monitoring tool. Indeed, a first opposite trend is observed when the amplitudes of the *Re(Z)* parameters extracted from the *EIS* (i.e. the *Lf-Re(Z)* and *Hf-Re(Z)* resistances intercepted on the *EIS* x-axis at low and high frequencies) are compared respectively with the $Lf\text{-}h_0$ and $Hf\text{-}h_0$ features estimated from the *VSS*. This first comparison suggests that it is possible to relate the shape and the morphology of the stack voltage signal (described through the *VSS* pattern and in particular by its h_0 feature) with different physical phenomena involved in the *FC* (linked with the shape of the *EIS* plot, and especially with the locations of *Lf-Re(Z)* and *Hf-Re(Z)* on the *EIS* Nyquist graphs).

On the basis of this first *VSS* - *EIS* comparison, a second and more detailed analysis is done to explore any possible relations existing between *Lf-Re(Z)* and $Lf\text{-}h_0$ on the one hand, and between *Hf-Re(Z)* and $Hf\text{-}h_0$ on the other hand. This last analysis is based on a data clustering process applied to the *Lf-Re(Z)*, $Lf\text{-}h_0$, *Hf-Re(Z)*, and $Hf\text{-}h_0$ parameters to generate some clusters related with different *FC* operating states (associated to the "normal", "poorer diffusion", "better diffusion", "lower *MEA* hydration", "better *MEA* hydration" labels). The results of the clustering indicate that the $Lf\text{-}h_0$ feature can be considered, almost like the *Lf-Re(Z)* parameter, to identify some *OC* related with the use of various cathode stoichiometry rates (inducing different air diffusion rates). To extrapolate, one can assume that

the *Lf-h_0* feature could also be used to detect any other low frequency phenomena (e.g. diffusion at anode) that were not taken into consideration in our study. The results of the clustering process also indicate that the *Hf-h_0* feature can potentially be considered, almost like the *Hf-Re(Z)* parameter, to identify some *OC* related with different hydration states of the *MEA*.

To conclude, with this work, we could establish some relations between the *VSS* patterns, computed from high and low filtered voltage signals, and the popular *EIS* signatures. We could also show that the dominant singularity strengths of the *Lf-VSS* (and possibly also the *Hf-VSS*) can be considered as relevant features to characterize and detect some *FC* operating states (e.g. lower / higher air diffusion, may be also lower / higher *MEA* hydration), as it is usually done with the use of characteristic points in the *EIS* plots (as the resistances intercepted on the *EIS* x-axis: *Lf-Re(Z)* and *Hf-Re(Z)*). Once more, the interest of using *VSS* features instead of *EIS* ones is that only the "free" evolution of the *FC* stack voltage can be considered and that there is no need of additional current excitation (as it is the case with the *EIS* applied in galvanostatic mode). Besides, the performing time of a full *VSS* computation is about 5 s (including the record of 10000 voltage samples at 3 kHz), against the duration of the *EIS* record that needs approximately 8 min in our study.

As an outlook and to complete the proposed diagnosis strategy presented in Fig. 1, it would be possible to conduct a work on the *FC* fault discrimination and detection using Machine Learning approaches. In that way, relevant singularity features extracted from the *Lf VSS* and *Hf-VSS* could be classified into different classes related to normal and abnormal *OC* with more complicated situations combining two or three *FC* faults occurring simultaneously, as it was already done in [25] but only on the basis of *VSS* recorded at a frequency of 11 Hz (and without applying any filtering process). It is expected that applying the new method described in this article will improve the classification of the *FC* operating states through the better differentiation of *FC* physical phenomena involving either low or high frequency dynamics.

Acknowledgments:

The work performed was done within the French ANR project, titled "Decentralized energy production", directed by EFFICACITY, the French R&D Institute for urban energy transition, and with IFSTTAR, the French institute of science and technology for transport, development and networks.

References:

[1] Hart D, Lehner F, Rose R, Lewis J, Klippenstein M. Fuel Cell Industry Review 2015, E4tech, Copyright: E4tech. 52 pages. November 2015. Link: http://wwwfuelcellindustryreview.com. (Last access: 10/11/2017).

[2] Ramesohl S. Callux - The German Lighthouse Project for Market Introduction for Domestic Fuel Cell CHP Systems. 4th IPHE Workshop Report Stationary Fuel Cells, Tokyo, 2011.

[3] AFHYPAC. Projet ene.field : un nouvel élan ! Gazette de l'Hydrogène 2013; 34: page 3. Link: http://enefield.eu/news/latest-news/gazette-de-lhydrogene-projet-ene-fi-eld-un-nouvel-elan/ (Last access: 10/11/2017).

[4] Manmeet Kaur, Kaushik Pal. Review on hydrogen storage materials and methods from an electrochemical viewpoint. Journal of Energy Storage 2019; 23:234–249.

[5] Lauinger D, Caliandro P, Van herle J, Kuhn D. A linear programming approach to the optimization of residential energy systems. Journal of Energy Storage 2016; 7:24-37.

[6] Rosato A, Sibilio S. Performance assessment of a micro-cogeneration system under realistic operating conditions. Energy Conversion and Management 2013; 70:149-162.

[7] Curtin S, Gangi J. Fuel Cell Technologies Market Report. U. S Department of Energy, 2015. 72 pages. Link: https://energy.gov/sites/prod/files/2016/10/f33/fcto_2015_market_report.pdf

[8] Bharathiraja B, Sudharsanaa T, Bharghavi A, Jayamuthunagai J, Praveenkumar R. Biohydrogen and Biogas – An overview on feedstocks and enhancement process. Fuel 2016; 185:810-828.

[9] Guan T, Alvfors P, Lindbergh G. Investigation of the prospect of energy self-sufficiency and technical performance of an integrated PEMFC (proton exchange membrane fuel cell), dairy farm and biogas plant system. Applied Energy 2014; 130:685-691.

[10] Mench M, Kumbur AC, Veziroglu TN. Polymer Electrolyte Fuel Cell Degradation. 1st Edition. USA: Academic Press; 2011. 472 pages.

[11] Polverino P, Sorrentino M, Pianese C. A model-based diagnostic technique to enhance faults isolability in Solid Oxide Fuel Cell systems. Applied Energy 2017; 204:1198-1214.

[12] Mainka J, Maranzana G, Thomas A, Dillet J, Didierjean S, Lottin O. One-dimensional Model of Oxygen Transport Impedance Accounting for Convection Perpendicular to the Electrode. Fuel Cells 2012; 12(5):848-861.

[13] Chevalier S, Auvity B, Olivier JC, Josset C, Trichet D, Machmoum M. Detection of Cells State-of-Health in PEM Fuel Cell Stack Using EIS Measurements Coupled with Multiphysics Modeling. Fuel Cells 2014; 14(3):416-429.

[14] Petrone R, Zheng Z, Hissel D, Péra MC, Pianese C, Sorrentino M, Becherif M, Yousfi-Steiner N. A review on model-based diagnosis methodologies for PEMFCs. Int J of Hydrogen Energy 2013; 38(17):7077-7091.

[15] Mao L, Jackson L, Dunnett D. Fault diagnosis of practical polymer electrolyte membrane (PEM) fuel cell system with data-driven approaches. Fuel Cells 2016; 17(2):247-258.

[16] Li Z, Giurgea S, Outbib R, Hissel D. Data-driven diagnosis of PEM fuel cell: A comparative study. Control Engineering Practice 2014; 28:1-12.

[17] Zheng Z, Morando S, Péra MC, Hissel D, Larger L, Martinenghi R, Fuentes AB. Brain-inspired computational paradigm dedicated to fault diagnosis of PEM fuel cell stack. Int J of Hydrogen Energy 2017; 42(8):5410-5425.

[18] Maizia R, Dib A, Thomas A, Martemianov A. Proton exchange membrane fuel cell diagnosis by spectral characterization of the electrochemical noise. J of Power Sources 2017; 342:553-561.

[19] Pahon E, Yousfi Steiner N, Jemeï S, Hissel D, Moçoteguy P. A signal-based method for fast PEMFC diagnosis. Applied Energy 2016; 165:748-758.

[20] Benouioua D, Candusso D, Harel F, Oukhellou L. Multifractal analysis of stack voltage based on wavelet leaders: A new tool for PEMFC diagnosis. Fuel Cells 2017; 17(2):217-224.

[21] D. Benouioua, D. Candusso, F. Harel, L. Oukhellou. Fuel cell diagnosis method based on multifractal analysis of stack voltage signal. Int J of Hydrogen Energy 2014; 39(5):2236-2245

[22] Benouioua D, Candusso D, Harel F, Oukhellou L. PEMFC stack voltage singularity measurement and fault classification. Int J of Hydrogen Energy 2014; 39(36):21631-21637.

[23] D. Benouioua, D. Candusso, F. Harel, L. Oukhellou. Multifractal Analysis of Stack Voltage Based on Wavelet Leaders: A New Tool for PEMFC Diagnosis. Fuel Cells 2017; 2(17):217-224.

[24] Benouioua D, Candusso D, Harel F, Oukhellou L. The dynamic multifractality in PEMFC stack voltage signal as a tool for the aging monitoring. Int J of Hydrogen Energy 2017; 42(2):1466-1471.

[25] D. Benouioua, D. Candusso, F. Harel, P. Picard, X. François. On the issue of the PEMFC operating fault identification: Generic analysis tool based on voltage pointwise singularity strengths. Int J of Hydrogen Energy 2018; 43(25):11606-11613.

[26] Becherif M, Péra MC, Hissel D, Zheng Z. Determination of the health state of fuel cell vehicle for a clean transportation. Journal of Cleaner Production 2018; 171:1510-1519.

[27] Hissel D, Candusso D, Harel F. Fuzzy-Clustering durability diagnosis of Polymer Electrolyte Fuel Cells dedicated to transportation applications. IEEE Transactions on Vehicular Technology 2007; 56(5):2414-2420.

[28] Kim J, Lee I, Tak Y, Cho BH. State-of-Health diagnosis based on hamming neural network using output voltage pattern recognition for a PEM fuel cell. Int J of Hydrogen Energy 2012; 37(5):4280-4289.

[29] Li Z, Outbib R, Giurgia S, Hissel D, Jemeï S, Giraud A, Rosini S. Online implementation of SVM based fault diagnosis strategy for PEMFC systems. Applied Energy 2016; 164:284-293.

[30] Rubio MA, Bethune K, Urquia A, St-Pierre J. Proton exchange membrane fuel cell failure mode early diagnosis with wavelet analysis of electrochemical noise. Int J of Hydrogen Energy 2016; 41(33):14991-15001.

[31] Cooper KR, Smith M. Electrical test methods for on-line fuel cell ohmic resistance measurement. J of Power Sources 2006; 160(2):1088-1095.

[32] Wang G, Wang K. Study and design of exponential and Butterworth low-pass filters used for digital speckle interference fringe filtering. Optik - International Journal for Light and Electron Optics 2013; 124(24):6713-6717.

[33] Mello RGT, Oliveira LF, Nadal J. Digital Butterworth filter for subtracting noise from low magnitude surface electromyogram. Computer methods and programs in Biomedecine 2007; 87(1):28-35.

[34] Challis RE, Kitney RI. The design of digital filters for biomedical signal processing. Part 2: Design techniques using the Z- Plane. J of Biomedical Engineering 1983; 5(1):19-30.

[35] Leonarduzzi R, Alzamendi G, Schlotthauer G, Torres M. Wavelet leader multifractal analysis of period and amplitude sequences from sustained vowels. Speech Communication 2015; 72:1-12.

[36] Barunik J, Aste T, Di Matteo T, Liu R. Understanding the source of multifractality in financial markets. Physica A 2012; 391(17):4234-4251.

[37] Kestener P, Conlon PA, Khalil A, Fennel A, McAteer RTJ, Gallagher PT, Arneodo A. Characterizing complexity in solar magnetogram data using a wavelet-based segmentation method. The Astrophysical Journal 2010; 717(2):995-1005.

[38] Jaffard S, Lashermes B, Abry P. Wavelet leaders in multifractal analysis, in Wavelet Analysis and Applications. Ed. Birkhäuser Verlag. 2006.

[39] Abry P, Goncalves P, Lévy-Véhel J. Lois d'échelle, Fractales et ondelettes. Eds. Hermès, 2002.

Figure captions:

Fig. 1. Synoptic diagram illustrating the two different steps of the proposed diagnostic strategy. This work deals with the step 1 of the global approach.

Fig. 2. Pictures of the investigated *PEMFC* stack designed for *μCHP* operation mode. Left: stack only. Right: stack instrumented and integrated in the testbench.

Fig. 3. Picture of the *PEMFC* teststand with its different sub-systems.

Fig. 4. Typical stack voltage signals of the studied *PEMFC* operated in normal and abnormal operating conditions, with f_s = 3 kHz.

Fig. 5. Stack voltage signal filtering process using two classes of *Butterworth filter*: a) original voltage signal, b1) high-pass filter frequency response and c1) the corresponding filtered voltage signal, b2) low-pass filter frequency response and c2) the resulting filtered signal.

Fig. 6. Typical curves of the stack voltage signal (left) and its corresponding *VSS* (right).

Fig. 7. Results of the *VSS* obtained for normal (Ref) and abnormal Operating Conditions (*OC*), for: a) raw voltage signals with *fs* =3 kHz, b) high and low filtered voltage signals (respectively *Hf-VSS* and *Lf-VSS*).

Fig. 8. Comparative study between *VSS* and *EIS* analysis tools.
Up: *VSS* results vs. *EIS* ones are represented for 6 *OC* of the *FC* (1 normal and 5 abnormal *OC*).
Middle: Bar diagram plots given for dominant singularity strengths from *Lf-VSS*, compared to low frequency resistances *Lf-Re(Z)* from *EIS* (*Lf* = [0.1 - 1] Hz).
Below: Bar diagram plots for dominant singularity strengths from *Hf-VSS*, compared to high frequency resistances *Hf-Re(Z)* from *EIS* (*Hf* = [1 - 1.5] kHz). Horizontal dashed lines (--) of the bar diagrams highlight both dominant singularity strength and resistance values resulting from the *FC* normal *OC*.

Fig. 9. For the 6 Operating Conditions (*OC*), plot of $Lf\text{-}h_0$, the dominant singularity strength measured on the *Lf-VSS*, as a function of *Lf-Re(Z)*, the resistance intercepted on the *EIS* x-axis at low frequency.
a) Up: clustering of the *OC* done from the *Lf-Re(Z)* data.
b) Down: clustering of the *OC* done from the $Lf\text{-}h_0$ data.

Fig. 10. For the 6 Operating Conditions (*OC*), plot of *Hf-*h_0, the dominant singularity strength measured on the *Hf-VSS*, as a function of *Hf-Re(Z)*, the resistance intercepted on the *EIS* x-axis at high frequency.

a) **Up**: clustering of the *OC* done from the *Hf-Re(Z)* data.

b) **Down**: clustering of the *OC* done from the *Hf-*h_0 data.

Table captions:

Table 1. Summary of the experimented stack characteristics and nominal operating parameters.

Table 2. The Operating Conditions (OC1, … , OC6) induced during the experimental campaign conducted with the investigated PEMFC. The parameter values in bold and underlined correspond to the introduced faults.